JOURNAL OF MECHANICAL ENGINEERING AND SCIENCES
ISSN: 2289-4659 e-ISSN: 2231-8380
VOLUME 19, ISSUE 4, 2025, 10877 - 10888
DOI: https://doi.org/10.15282/jmes.19.4.2025.4.0852

RESEARCH ARTICLE

The impact of baffle configuration on the performance of a shell-and-tube heat exchanger using the Bell-Delaware approach

M. Saif*, M. Tariq

Department of Mechanical Engineering, Sam Higginbottom University of Agriculture, Technology and Sciences (SHUATS), Prayagraj, 211007, Uttar Pradesh, India

ABSTRACT - Shell-and-tube heat exchangers (STHXs) are frequently used across industries. Their performance is determined by the thermal and hydraulic characteristics, which depend on inlet conditions, flow conditions, and the geometry of the shell and tubes bundle. A computational model was generated to solve the governing equations, utilising Microsoft Excel 2016. The program predicts the performance of the STHX for shell-side heat transfer coefficient (h_s), pressure loss (ΔP_s) and the performance ratio ($h_s/\Delta P_s$) by employing the Bell-Delaware method. This method showed the best reliability against experimental results. The aim of the study is to analyse the influence of variations in baffle number, baffle cuts, tube layouts, six fluid characteristics, and mass flow rate. The findings of the investigation indicate that the heat transfer coefficient and pressure loss increase, while the value of ($h_s/\Delta P_s$) decreases as the baffle number increases for all the tube layouts. The h_s and ΔP_s decrease with increasing baffle cuts for all layouts. A baffle count of six exhibits the highest value of ($h_s/\Delta P_s$) for all the fluids and layouts. The rotated square tube arrangement yields higher h_s and moderate ΔP_s, which in turn yields the highest ($h_s/\Delta P_s$) ratio compared to triangular and square layouts.

ARTICLE HISTORY
Received : 29th Apr. 2025
Revised : 23rd Sept. 2025
Accepted : 26th Oct. 2025
Published : 29th Dec. 2025

KEYWORDS
Baffle cuts
Heat transfer coefficient
Pressure loss
($h_s/\Delta P_s$) ratio
STHX
Tube layouts

1. INTRODUCTION

A shell-and-tube heat exchanger (STHX) is extensively used in industries due to its high thermal efficiency, durability, and ability to handle high-pressure applications [1]. It consists of a cylindrical shell housing a bundle of tubes through which one fluid flows, while another fluid flows over the tubes within the shell, enabling effective heat transfer. To enhance thermal performance, segmental baffles are introduced inside the shell to guide the shell-side fluid in a zigzag pattern, increasing turbulence and thus improving heat transfer rates. These baffles help minimise stagnant zones and promote better heat exchange; however, they also contribute to increased pressure loss. STHXs with segmental baffles are commonly utilised in industries, such as power generation, chemical processing and oil refining, due to their robust design and efficient thermal management [2].

The Tubular Exchanger Manufacturers Association (TEMA) standards are widely followed for designing STHXs, combining classes R, C, and B into a single section titled Class RCB. The key factors affecting shell-side performance include baffle number, baffle cuts, tube layouts, mass flow rate, flow types and fluid properties such as density, specific heat, viscosity, and thermal conductivity [3].

Analysing the performance of an STHX involves a variety of calculations, and several algorithms have been employed in recent years. The key algorithms and methods used include genetic algorithms (GA), particle swarm optimisation, finite difference/volume method, HTRI Xchanger suite, COMSOL Multiphysics, computational fluid dynamics (CFD), logarithmic mean temperature difference (LMTD), ε-NTU, Kern and the Bell-Delaware (B-D) approach. Among these, Kern and the B-D method are preferred for basic thermo-hydraulic calculations. However, the B-D method, though more complex, provides greater accuracy in predicting shell-side heat transfer and pressure loss by accounting for flow patterns and leakage through baffles, making it a superior choice for detailed analysis. In many studies, calculations from the B-D method show good agreement with experimental and simulation results.

Various authors have explored these optimisation techniques and numerical methods to enhance thermal efficiency and reduce costs, analysing design parameters such as baffle configurations, tube layouts, and pressure loss constraints to improve performance. Several past studies are discussed below:

Ozden and Tari [4] examined the effects of shell-side parameters like baffle number, baffle cut, and shell diameter on heat transfer capacity and pressure loss in small STHX using CFD simulations. CFD results are validated by comparing them with the B-D method for accuracy. Similarly, Uosofvand *et al.* [5] observed the performance of a small STHX using CFD. The baffle orientations are investigated, showing that a 90° orientation enhances performance. Results align well with the B-D method and experimental data. Further, Alperen *et al.* [6] examined the results of HTRI Xchanger software, Kern, and B-D methods for analysing STHXs against experimental data. The shell-side heat transfer coefficient (h_s) showed deviations of +17%, -11%, and +18%, while pressure loss (ΔP_s) deviations were +64%, -25%, and -32%, by

***CORRESPONDING AUTHOR | M. Saif** | ✉ saifmech08@gmail.com

Kern, B-D methods and HTRI Xchanger program respectively. In addition, Lara-Montano *et al*. [7] optimised the STHXs through four case studies, applying Kern and B-D methods with discrete and continuous tube diameters. A total of 16 optimisation problems are analysed, minimising total annual cost. Seven metaheuristic algorithms are used to solve each optimisation problem efficiently. In addition, Xu *et al*. [8] established a B-D based prediction model for shell-and-tube heat exchanger with segmental baffles (SHTX-SB) to analyse tube parametric effects on heat transfer efficiency and adopted algorithm techniques for optimisation to enhance heat transfer capacity per pressure loss and weight, improving design reliability. Moreover, Kotian *et al*. [9] compared the Colburn and B-D method for evaluating an STHX performance by varying hot side temperatures to analyse heat load, heat transfer coefficient, and effectiveness, concluding that the B-D is more reliable due to its consideration of practical losses. In addition, Jamil *et al*. [10] optimised an STHX design using numerical approaches. A numerical model analysed thermal, hydraulic, exergy, and economic aspects. Normalised sensitivity analysis and GA identify key parameters. The calculations using the Wills-Johnston method closely match those of the B-D method. Furthermore, Suliman Alfarawi [11] studied an STHX performance using 3D CFD analysis in COMSOL Multiphysics by considering the impacts of segmental baffle cuts and baffle numbers on hydro-thermal performance at varying Reynolds numbers, highlighting CFD, Kern and LMTD's role in heat exchanger modelling. In addition, Mami *et al*. [12] modelled a heat exchanger for an LPG production unit using the B-D and Taborek methods, optimising geometric parameters. Results show good agreement with real data, validating the calculations of the heat transfer coefficient. Although authors have examined STHX performance parameters to enhance heat transfer efficiency and minimise pressure drop by adopting the B-D method, mathematical correlations, and CFD simulations—most studies have focused on baffle spacing, cuts, and orientations. The B-D method shows better agreement with the CFD results. The experimental and CFD results confirm that baffles significantly influence shell-side flow [13-17].

Additionally, a report with a new analysis approach presented by Sarmiento *et al*. [18] analysed a two-phase thermosyphon-assisted shell-and-tube heat exchanger through theoretical modelling and experiments. A prototype was tested for oil cooling, integrating the B-D method, an equivalent thermal circuit model, and a novel thermal coupling algorithm for heat transfer prediction. Further, McCaughtry and Kim [19] sought to enhance the teaching-learning-based optimisation (TLBO) algorithm for improved heat exchanger design feasibility. The updated TLBO and B-D method are validated against real cases, analysing parameter impacts on performance and optimal design. Moreover, Han *et al*. [20] developed a comprehensive thermal-economic model for STHXs using Kern and B-D methods based on LMTD and ε-NTU approaches. It introduces an improved sparrow search algorithm to optimise the economic-based thermal design to enhance the efficiency. In addition, Yang *et al*. [21] developed an automated optimisation model for sizing shell-and-tube horizontal thermosyphon reboilers using global optimisation to enhance thermal performance across various applications. The B-D, Aspen EDR and Nitsche's methods validate the findings. Also, Prajapati *et al*. [22] analysed and optimised a water–water STHX with segmental baffles by considering shell-and-tube side variables. Using the Kern method, heat transfer search algorithm, and TOPSIS, the exchanger is optimised for minimal cost and maximum efficiency. Additionally, several studies have focused on optimising the STHXs using various baffle designs. Various authors explored the STHX-SB using trefoil-hole baffles, pseudohelical baffles, STHX with staggered baffles (STHX-ST), STHX-SB using ribbed tubes and combined baffle configurations, a novel helical baffle design with segmental baffles, a novel STHX with segmental porous baffles, STHX with a quatrefoil perforated plate (QPP) support structure, a segmented trefoil baffle (STB) and new STHX with inclined-segmental baffles, respectively. Studies evaluated performance based on metrics like heat transfer coefficient, pressure loss, fouling resistance, and thermo-hydraulic performance. Researchers employed CFD simulations, machine learning and multi-objective optimisation techniques. The results were validated against experimental data, numerical results from other studies, and established methods like the B-D, ensuring the accuracy of the simulations [23-31]. Besides this, certain scholars have adopted different working fluids. Research conducted by Xiao *et al*. [32] examined the heat transfer and fluid flow performance of heat exchangers with different baffle tilt angles and different fluids using CFD analysis. It highlights performance comparison under equal heat transfer capacity and examines baffles, exchanger length, and Prandtl number. In addition, authors [33-35] studied the performance of an STHX with various baffle configurations by utilising engineering equation solver (EES) software and the B-D formulas for segmental baffles and mathematical correlations for helical baffles. The B-D method was most accurate with the square and rotated square tube layouts offering the highest heat transfer efficiency. Furthermore, Abd *et al.* [36] examined the impact of shell diameter, tube length, baffle spacing and cutting space on heat transfer and pressure loss in an STHX with triangular and square pitches. It also considers fouling effects on shell-and-tube sides, providing insights for efficient heat exchanger design.

The reviewed literature explores various optimisation and numerical techniques for enhancing the STHX performance. Several researchers inspected the influence of baffle numbers, cuts, orientations, and tube layouts on the performance, confirming that optimised shell-side configurations improve heat transfer while reducing pressure loss. Many studies validate CFD simulations using Kern, mathematical correlations, algorithms and the B-D method, which is preferred for its accuracy in predicting shell-side heat transfer and pressure loss. Further, studies analyse different working fluids with selective parameters and their thermal-hydraulic effects, emphasising optimisation for improved exchanger performance across various industrial applications. Hence, this research aims to analyse the execution of an STHX-SB implementing the B-D approach and validated with the experimental data reported in the literature, considering the impacts of shell-side design parameters with the six different fluid properties and tube layouts for finding the best results with respect to the heat transfer coefficient, pressure loss and the ratio of ($h_s/\Delta P_s$).

2. MATERIALS AND METHODS

This section details the heat exchanger type, its construction and geometric details, working fluid utilised with their thermo-hydraulic properties, software and the B-D method for validation and computational purposes. All the information regarding the input parameters is listed below:

i) The outcomes of the experimental investigation performed by Chen *et al.* [27] were taken into consideration during this analysis. A TEMA E-type STHX with one shell pass and single pass fixed tube sheet with shell-side design as a 30% baffle cut and segmental baffles is adopted in this study.

ii) The shell-side h_s and ΔP_s values have been evaluated and compared with the experimental results.

iii) The heat exchanger dimensional attributes are presented in Table 1.

iv) The six different types of working fluid are taken into account for computation purposes, which are ethylene glycol, kerosene oil, light crude oil, gasoil, glycerine and engine oil [2, 27].

v) The thermo-hydraulic properties, like density (ρ), specific heat (c_p), viscosity (μ), and thermal conductivity $(k)$of the fluids have been selected for the analysis and their values are shown in Table 2.

vi) The mathematical formulas and correlations for the B-D approach have been executed in MS Excel 2016.

Table 1. Structural parameters of the STHX-SB

Item	Unit	Value
Heat exchanger type		ASME E
Shell inside diameter (D_s)	m	0.144
Shell outside diameter (D_o)	m	0.159
External diameter of tube (d_o)	m	0.016
Internal diameter of tube (d_i)	m	0.015
Tube pitch (P_t)	m	0.019
Overall tube length (L)	m	1.051
Number of tubes (N_t)		19
Tube layout angle (θ_{tp})	Degree (°)	30
Number of baffles (N_b)		12
Baffles thickness (t_b)	m	0.005
Baffle spacing (L_{bc})	m	0.0875
Baffle cut (B_c)	%	30
Material		Stainless steel
Flow direction		Counter flow

Table 2. Thermo-hydraulic properties of the six fluids

Working fluids	Ethylene glycol	Kerosene oil	Light crude oil	Gasoil	Glycerine	Engine oil
Density (ρ), (kg/m^3)	1079.0	891.45	801.05	815.0	1230.0	853.9
Specific heat (c_p),(J/kg.K)	2637.0	2198.8	2087.89	2100.0	2427.0	2119.0
Viscosity (μ), (Pa.s)	0.00342	0.00084	0.0024	0.0025	0.05	0.03915
Thermal conductivity(k), (W/m.K)	0.261	0.142	0.1412	0.135	0.292	0.138

2.1 The Bell-Delaware method

The B-D method is a widely applied approach for computing the h_s and ΔP_s in an STHX. It considers various parameters, including shell-side and tubeside to enhance accuracy. This method acknowledges that only a portion of the shell-side fluid flows perpendicularly across the tubes, while the rest moves through bypass areas, following the path of least resistance. In typical designs, up to 40% of the total flow follows these non-ideal paths, significantly influencing the heat transfer capacity and pressure loss phenomena. To account for these effects, the total fluid flow is divided into several distinct streams.

These fluid streams in an STHX are ranked based on their thermal effectiveness. The A stream (tube to baffle hole leakage) is the most effective, as high heat transfer occurs in the annular spaces. The B stream (cross flow through the tube bundle) is also completely efficient for the outcomes h_s and ΔP_s. The C stream (bypass for bundle to shell) is only partially effective, as it flows around the perimeter of the tube bundle. The E stream (leakage for shell to baffle) is the

least effective, especially in laminar flow. The F stream (bypass for tube pass partition) forms due to open passages in multipass units, as shown in Figure 1 [3, 33].

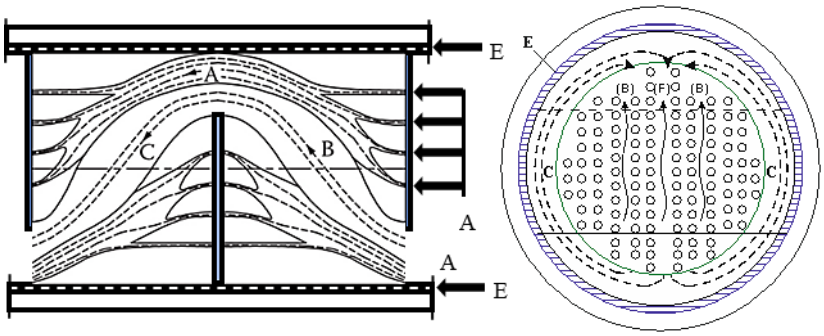

Figure 1. Illustrates various stream flows within the tube bundle

2.1.1 The shell-side parameters

For a fixed tube sheet heat exchanger, bundle to shell clearance (L_{bb}) is given by Eq. (1):

$$L_{bb} = 12 + D_s \tag{1}$$

The bundle diameter (D_{ctl}) is evaluated from the Eq. (2):

$$\begin{aligned} D_{otl} &= D_s - L_{bb} \\ &= D_{ctl} - d_o \\ D_{ctl} &= D_{otl} - d_o \end{aligned} \tag{2}$$

where, d_o is the tube outside diameter.

2.1.2 The auxiliary calculations

These are the additional relations which are applicable in B-D method for determining the h_s and ΔP_s.

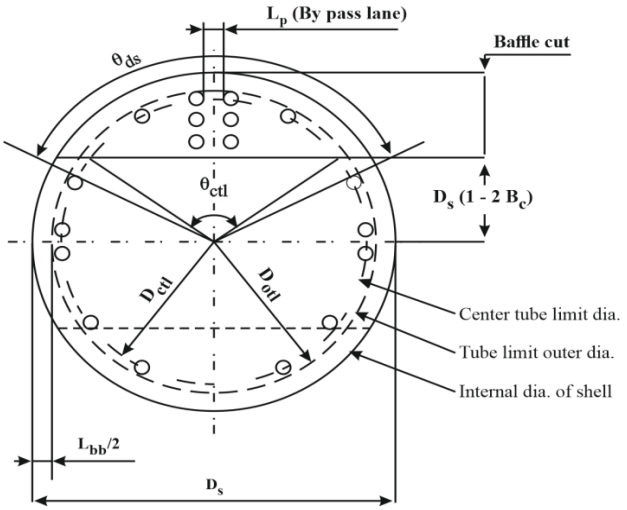

Figure 2. Basic configuration of segmental baffles

The central angle of a baffle cut (θ_{ds}), as illustrated in Figure 2, is expressed by Eq. (3):

$$\theta_{ds} = 2.\cos^{-1}(1 - 2.B_c) \tag{3}$$

The upper central angle of the baffle cut (θ_{ctl}) as illustrated in Figure 2. It is defined by Eq. (4):

$$\theta_{ctl} = 2.\cos^{-1}\left[\frac{D_s.(1 - 2.B_c)}{D_{ctl}}\right] \tag{4}$$

The cross-flow area for shell-side (S_m) is given by Eq. (5):

$$S_m = L_{bc}.\left[L_{bb} + \frac{D_{ctl}.(P_t - d_o)}{P_n}\right] \tag{5}$$

Here P_n represents the tube pitch perpendicular to the shell cross-flow and P_t is tube pitch.

Also $P_n = P_t$ for 30° and 90° tube layouts
$= (0.707.P_t)$ for 45° tube layouts

The total area for window flow (S_{wg}) is given by Eq. (6):

$$S_{wg} = \frac{1}{8}.D_s^2.(\theta_{ds} - \text{Sin}\,\theta_{ds}) \tag{6}$$

Further, to estimate the tubes fractions in baffle window (F_w) and in an absolute cross-flow(F_C), as shown in Figure 2 by a distance of $D_s.(1-2.B_c)$ is given by Eq. (7):

$$F_c = 1 + \frac{1}{\pi}[\sin\theta_{ctl} - \theta_{ctl}] \tag{7}$$

Similarly, the tube number in the window (N_{tw}) is expressed by Eq. (8):

$$N_{tw} = N_t.F_w \tag{8}$$

where, $F_W = \frac{1}{2\pi}[\text{Sin}\,\theta_{ctl} - \theta_{ctl}]$

The window area for the segmental baffle filled by the tube (S_{wt}) is given by Eq. (9):

$$S_{wt} = N_{tw}.\frac{\pi}{4}{d_o}^2 \tag{9}$$

The net cross-flow area through one baffle window (S_w) is given by Eq. (10):

$$S_w = S_{wg} - S_{wt} \tag{10}$$

The total number cross-flow section of tube rows effectively crossed in single cross-flow section (N_{tc}) i.e. between the baffle tips is expressed by Eq. (11):

$$N_{tc} = \frac{D_s.(1-2.B_c)}{P_p} \tag{11}$$

where P_p stands for the tube pitch on the cross-flow direction.

$P_p = (0.866.P_t)$ For 30° tube layout
$= (0.707.P_t)$ For 45° tube layout
$= P_t$ For 90° tube layout

and the effective tube rows number crossed in the baffle window (N_{cw}) is expressed by Eq. (12):

$$N_{cw} = \frac{0.8.B_c.D_s}{P_p} \tag{12}$$

The bundle to shell by pass area (S_b) is expressed by Eq. (13):

$$S_b = L_{bc}.(D_s - D_{otl}).(D_s - D_{otl}) \tag{13}$$

This is for no tube partition width i.e. for single pass.

The leakage area between the shell and a single baffle (S_{sb}) is expressed by Eq. (14):

$$S_{sb} = D_s.L_{sb}.(1.571 - 0.0044.\theta_{ds}) \tag{14}$$

where L_{sb} refers to the gap between the shell and the baffle plate.

The leakage area between the tube and a single baffle (S_{tb}) is calculated by Eq. (15):

$$S_{tb} = \frac{\pi.d_o.L_{tb}.N_t.(1-F_w)}{2} \tag{15}$$

where L_{tb} is the gap between the tube surface and the edge of the tube hole. Its value ranges between 0.8 to 0.4.

The cross-flow velocity for shell-side (U_s) and mass flow rate $(m_s)$is denoted by Eq. (16):

$$U_s = \frac{m_s}{\rho_s.S_m} \tag{16}$$

where, m_s= Shell-side mass flow rate (kg/s).
ρ_s = The shell-side fluid density (kg/m^3).

2.1.3 The shell-side heat transfer and pressure loss correction factors:

In the B-D method, the flow fraction for each stream is determined based on its respective flow area and resistance. The heat transfer coefficient (h_s) for ideal crossflow is then adjusted using correction factors to account for the influence of each stream. The shell-side h_s is expressed by Eq. (17):

$$h_s = h_{id}.J_c.J_l.J_b.J_s.J_r \tag{17}$$

where h_{id} is the h_s for pure cross-flow of an ideal tube bank.

The segmental baffle window correction factor (J_c), for the baffle cut range 15 to 45% is expressed by Eq. (18):

$$J_c = 0.55 + 0.76.F_c \tag{18}$$

In a heat exchanger that's optimally designed with liquid on the shell-side, its typical value is around one.

The correction factor for baffle leakage effects for heat transfer (J_l) is expressed by Eq. (19):

$$J_l = 0.44.(1 - r_s) + [1 - 0.44.(1 - r_s)].\exp(-2.2.r_l) \tag{19}$$

where, $r_s = \frac{S_{sb}}{S_{sb}+S_{tb}}$, $r_l = \frac{S_{sb}+S_{tb}}{S_m}$

The adjustment factors for heat transfer due to bundle bypass effects (J_b). To calculate J_b by Eq. (20), the required parameters include the number of sealing strips and the number of tubes in the cross-flow area.

$$J_b = \exp\left\{-C_j.(F_{sbp}).\left[\left(1 - (2.r_{ss})\right)^{(1/3)}\right]\right\} \text{ For, } r_{ss} \le 0.5 \tag{20}$$

where, $J_b = 1$ for $r_{ss} \ge 0.5$ and $F_{sbp} = \frac{S_b}{S_m}$

For, $R_e \le 100 \Rightarrow C_j = 1.35$ and

$R_e > 100 \Rightarrow C_j = 1.25$.

The heat transfer correction factor for unequal baffle spacing at inlet and outlet (J_s) is expressed by Eq. (21):

Here, $J_s = 1$, in a heat exchanger where the spacing between all baffle plates is uniform.

Otherwise,

$$J_s = \frac{(N_b - 1) + \left(\frac{L_{bi}}{L_{bc}}\right)^{1-n_1} + \left(\frac{L_{bo}}{L_{bc}}\right)^{1-n_1}}{(N_b - 1) + \left(\frac{L_{bi}}{L_{bc}}\right) + \left(\frac{L_{bo}}{L_{bc}}\right)} \tag{21}$$

For, $R_e \ge 100, \Rightarrow n_1 = 0.6$ and $R_e < 100, \Rightarrow n_1 = 1/3$

The correction factor for heat transfer in laminar flow with adverse temperature gradient (J_r) is given by $J_r = 1$ for $R_e > 100$.

Now, the h_{id} is given by Eq. (22):

$$h_{id} = J_{id}c_{ps}.\left(\frac{m_s}{S_m}\right).\left(\frac{k}{\mu.C_p}\right)^{2/3}.\left(\frac{\mu}{\mu_w}\right)^{0.14} \tag{22}$$

Here, $G_s = \frac{m_s}{S_m}$, $P_r = \frac{\mu.C_p}{k}$ and $\emptyset_s = \frac{\mu}{\mu_w}$

where, $\emptyset_s$ is the viscosity correction factor addresses the change in a fluid's viscosity due to the temperature difference between the tube wall (μ_w) and the bulk fluid (μ).

Now, the non-dimensional thermal factor (J_{id}) in the ideal cross-flow is evaluated by Eq. (23) [6, 33]:

$$J_{id} = a_1.\left(\frac{133.d_o}{P_t}\right)^a.(R_e)^{a_2} \tag{23}$$

where, $a = \frac{a_3}{1+0.14.(R_e)^{a_4}}$

2.1.4 The pressure loss calculations with the Bell-Delaware method

The shell-side ΔP_s is calculated by adding all the losses for the intake and outlet sections and the internal sections after considering several correction factors as shown in Figure 3.

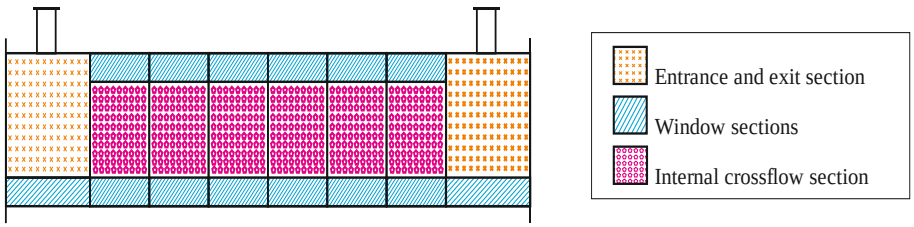

Figure 3. Factors contributing to pressure loss (shell-side) in a STHX

The total shell-side ΔP_s consists of all the losses due to (1) cross flow ΔP_c (2) window regions ΔP_w and (3) entrance and exit section on ΔP_e is given by Eq. (24):

$$\Delta P_s = \Delta P_c + \Delta P_w + \Delta P_e \tag{24}$$

The correction factor for baffle leakage effects (R_l) is expressed by Eq. (25):

$$R_l = \exp[-1.33(1 + r_{ss}).r_l^p] \tag{25}$$

The correction factor for bundle bypass effects (R_b) is expressed by Eq. (26):

If, $r_{ss} < 0.5$, then

$$R_b = \exp\left\{-C_r.\left(F_{sbp}\right)\left[\left(1-(2.r_{ss})\right)^{(1/3)}\right]\right\} \quad (26)$$

here, for, $R_e \leq 100 \Rightarrow C_r = 0.45$
and, $R_e > 100 \Rightarrow C_r = 3.7$.

Further, for $r_{ss} \geq 0.5$, R_b is assumed equal to 1.

The correction factor for unequal baffle spacing at the inlet and outlet (R_s) is given by Eq. (27):

$$R_s = \left[\left(\frac{L_{bc}}{L_{bi}}\right)^{(2-n_2)} + \left(\frac{L_{bc}}{L_{bo}}\right)^{(2-n_2)}\right] \quad (27)$$

for, $R_e \leq 100 \Rightarrow n_2 = 0.2$
and, $R_e > 100 \Rightarrow n_2 = 1$.

where, L_{bi} and L_{bo} are the distance for the baffle plates at the intake and exit sections, L_{bc} distance between the baffles as shown in Figure 4. Otherwise $R_e = 2$, when $L_{bi} = L_{bo} = L_{bc}$.

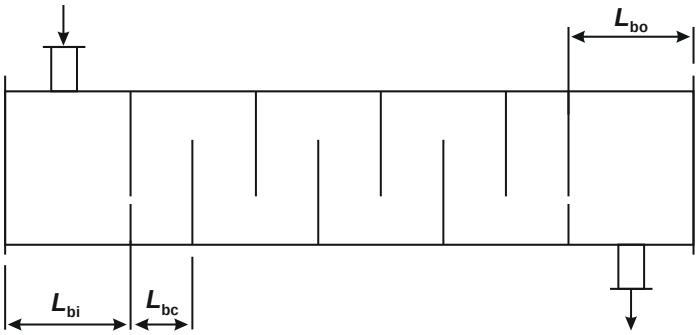

Figure 4. Standard arrangement of baffle spacing

Now, the pressure loss value in the cross-flow among all the central baffle plates (ΔP_c) is given by Eq. (28):

$$\Delta P_c = (N_b - 1).\Delta P_{ideal}.R_l.R_b \quad (28)$$

where, $(N_b - 1)$ is the number of cross flow zones, and $\Delta P_{ideal} = \frac{2f_{id}.N_c.G_s^2}{\rho}.\left(\frac{\mu_w}{\mu}\right)^{0.14}$ For, $R_e > 100$
where, the friction factor (f_{id}) for an ideal tube bundle is determined by Eq. (29):

$$f_{id} = b_1.\left(\frac{133.d_o}{P_t}\right)^b.(R_e)^{b_2} \quad (29)$$

where, $b = \frac{b_3}{1+0.14.(R_e)^{b_4}}$
The pressure loss in the window zone (ΔP_w) is given by Eq. (30):

$$\Delta P_w = N_b.\Delta P_{w,id}.R_l \quad (30)$$

where, $\Delta P_{w,id} = \frac{[2+0.6.N_{cw}].{m_s}^2}{2.g_c.\rho.S_m.S_w}$

and, the pressure loss in the shell intake and outlet sections (ΔP_e) is expressed by Eq. (31):

$$\Delta P_e = 2.\Delta P_{ideal}.\left(1+\frac{N_{cw}}{N_c}\right).R_b.R_s \quad (31)$$

Therefore, ΔP_s calculation can be done by putting the values of ΔP_c, ΔP_w and ΔP_e in the Eq. (24).

3. RESULTS AND DISCUSSION

3.1 The model validation

The experimental data from Chen *et al.* (2019) has been utilised to verify the numerical results of the present study at various mass flow rates. The STHX data is summarised in Table 1. The experimental findings are contrasted with predictions from the B-D method, a widely applied approach in heat exchanger designs. As shown in Figure 5(a) and Figure 5(b), the average deviations between the experimental outcomes and the B-D method concerning the h_s and ΔP_s on the shell-side are approximately 10% and 7%, respectively. These findings confirm the reliability of both the experimental setup and data processing methodology. Furthermore, Figure 5(a) indicates that the model tends to over-predict compared to the experimental data [27].

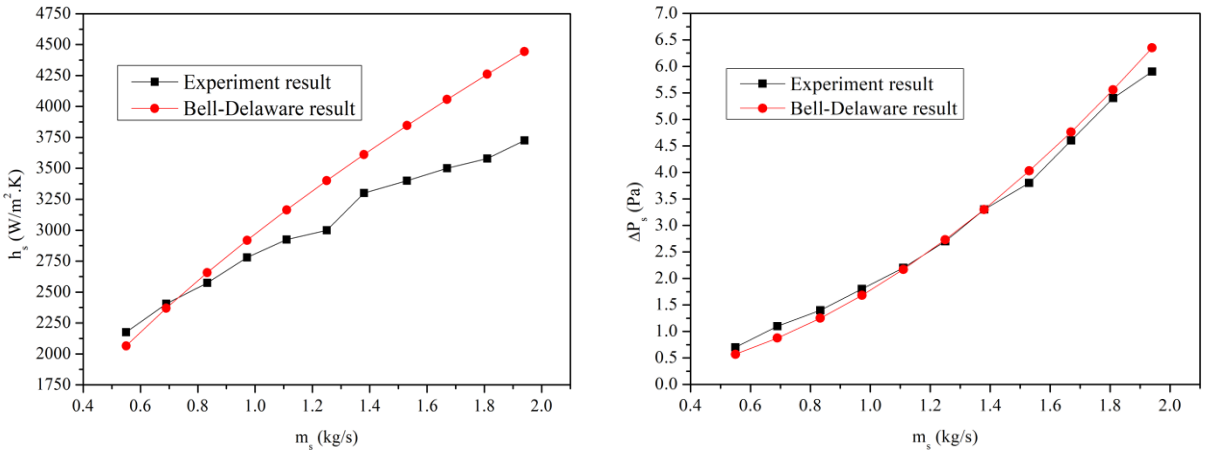

(a) (b)

Figure 5. Comparison of experimental and B-D results: (a) for h_s, and (b) ΔP_s

3.2 The Effects of The Tube Layouts in a STHX

The tube layout in a STHX affects thermal performance, pressure drop, and maintenance. The selection is determined by heat transfer requirements, pressure constraints, and fluid properties, ensuring optimal exchanger performance. The three main layouts are triangular (30°), square (90°), and rotated square (45°). The triangular layout maximises tube density, enhancing heat transfer through turbulence, but increases pressure loss. The square layout allows easier cleaning and lowers shell-side pressure loss, making it ideal for high-fouling fluids but with lower heat transfer efficiency. The rotated square layout offers a balance between heat transfer and maintenance accessibility, providing moderate thermal performance for applications requiring both efficiency and cleanability. Figure 6, Figure 7 and Figure 8 illustrate the effects of 30°, 45°, and 90° tube layouts for six different fluids on heat transfer coefficient, pressure loss and the ratio of ($h_s/\Delta P_s$) at varying numbers of baffles by employing the B-D method [37].

Figure 6 shows that an increase in the baffle numbers in a triangular layout (for m=3.5 kg/s, and B_c =25%) leads to a rise in the h_s and ΔP_s. Ethylene glycol has the highest h_s, while engine oil has the least h_s. Further, engine oil has the highest-pressure loss, while ethylene glycol has the least. Additionally, as the number of baffles decreases, the ratio of ($h_s/\Delta P_s$) increases for all fluids, but it is highest for ethylene glycol at $N_b = 6$. It has also been noticed that from $N_b = 6$ to 12, there is a smooth rise (16.24%) in h_s, but a sharp rise (260.42%) in pressure loss has been observed.

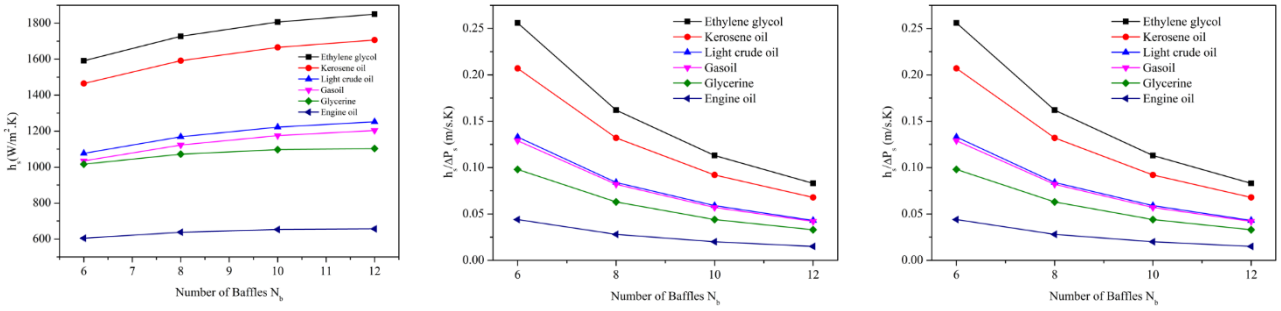

(a) (b) (c)

Figure 6. Impact of baffle numbers: (a) for h_s, (b) ΔP_s and (c) the ratio of ($h_s/\Delta P_s$)

Figure 7 shows the impact of the number of baffles in a rotated square layout. It is evident from the outcomes that similar trends are noticed for the fluids in terms of h_s, ΔP_s and the ratio of ($h_s/\Delta P_s$) as noted in the triangular layout. Likewise, it has also been noticed that from $N_b = 6$ to 12 there is a smooth rise (20.88 %) in h_s, but a sharp rise (265.51 %) in pressure loss has been observed. For Figure 6 and Figure 7, increasing the number of baffles enhances crossflow segments and tube fluid contacts, promoting turbulence and minimising dead zones, which improves h_s. Since ΔP_s is directly proportional to N_b, each additional baffle adds linearly to flow resistance, causing pressure drop to rise steadily. In contrast, the heat transfer coefficient increases mainly through enhanced turbulence, which saturates after moderate baffle numbers. Thus, beyond 6–8 baffles, the pressure drop penalty grows disproportionately larger than the marginal heat transfer gain. Among the fluids, ethylene glycol achieves the highest h_s, followed by kerosene, light crude oil, gas oil, glycerine, and engine oil. Engine oil records the highest ΔP_s due to its high viscosity, while ethylene glycol and kerosene maintain relatively lower ΔP_s because of lower viscosity and easier flow. Thus, ethylene glycol exhibits the highest ($h_s/\Delta P_s$) ratio, whereas engine oil shows the lowest ($h_s/\Delta P_s$) ratio. Additionally, fewer baffles (6–8) yield the highest ($h_s/\Delta P_s$) ratio, particularly for ethylene glycol and kerosene. For high viscosity fluids, additional baffles are inefficient but fewer baffles are more effective.

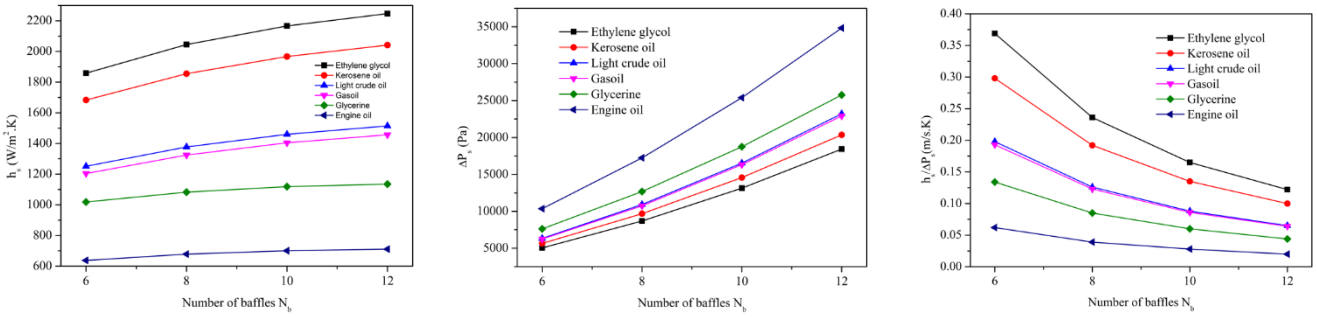

(a) (b) (c)

Figure 7. Shows impact of baffle numbers: (a) for h_s, (b) ΔP_s, and (c) the ratio of ($h_s/\Delta P_s$)

Figure 8 shows that a rise in the baffle numbers for a square layout leads to a rise in the h_s and ΔP_s. Here, kerosene oil has the highest h_s as compared to ethylene glycol, while engine oil has the least h_s. Since the kerosene oil's lower viscosity and associated enhancement in turbulence, combined with the geometric benefits of a square tube layout, results in a higher h_s relative to ethylene glycol and simultaneously increase frictional pressure losses too. Further, engine oil has the highest-pressure loss while ethylene glycol has the least. Additionally, as the number of baffles decreases, the ratio of ($h_s/\Delta P_s$) enhances for all fluids but it is highest for kerosene oil at $N_b = 6$. Likewise, it has also been noticed that from $N_b = 6$ to 12, there is a smooth rise (26.28 %) in h_s, but a sharp rise (266.88 %) in pressure loss has been observed.

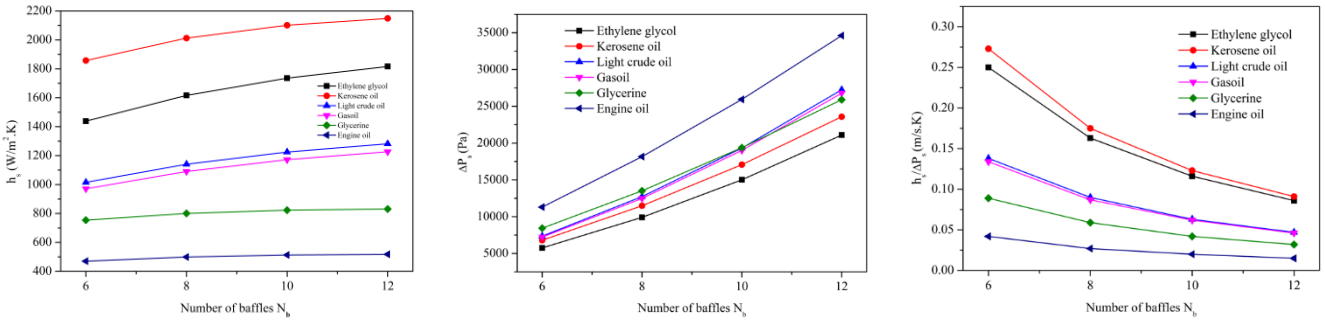

(a) (b) (c)

Figure 8. Shows impact of baffle numbers: (a) for h_s, (b) ΔP_s, and (c) the ratio of ($h_s/\Delta P_s$)

Moreover, Figure 9 exhibits the values of ($h_s/\Delta P_s$) ratios for the six considered fluids and three tube layouts. The graph patterns clearly indicate that the performance of the 45° tube layout is far better as compared with 30° and 90° tube layouts under the similar geometrical and operating circumstances.

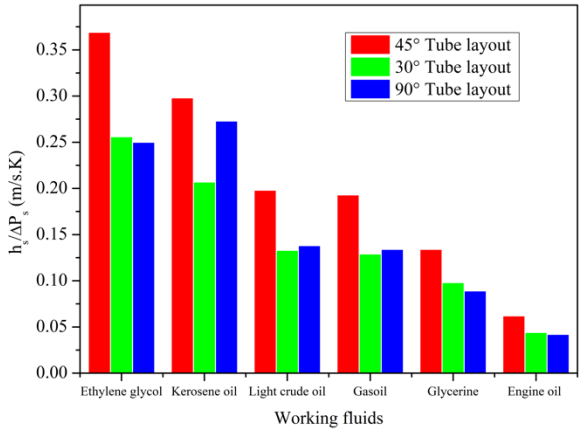

Figure 9. Shows the values of ($h_s/\Delta P_s$) ratio for all the fluids and tube layouts

3.3 The Effects of The Baffle Cuts in a STHX

The baffle cuts are openings in baffle plates that control shell-side fluid flow, influencing heat transfer and pressure loss. They direct fluid flow, reduce dead zones, and enhance turbulence for better heat exchange. Larger cuts means lower pressure loss but may reduce heat transfer, while smaller cuts increase turbulence but raise pressure loss. Baffle cuts normally range between 15 to 45% but the optimum values of baffle cut deviate between 22 to 35% inside diameter of the shell [3].

Figure 10, illustrates the effect of baffle cut variations on the h_s, ΔP_s and the ratio of ($h_s/\Delta P_s$) for the 30°, 45° and 90° tube layouts (for m_s = 3.5 kg/s and N_b=6). It is evident that as the baffle cuts increase, the h_s and ΔP_s reduce for all

the layouts. Additionally, the maximum value of h_s and ΔP_s are attained at smaller cut i.e. 22%, while the lowest value at higher cut i.e. 40%. Further, the value of ($h_s/\Delta P_s$) is highest for the 45°, followed by 90° and lowest for 30° layouts. The highest values of the ($h_s/\Delta P_s$) are at 35%, 30% and 40% baffle cuts for 45°, 90° and 30° layouts respectively. Therefore, the analysis reveals that the performance of 45° layout is better at all baffle cuts when compared with other layouts. The reason is that the 45° tube layout consistently achieves the highest h_s across all baffle cuts due to enhanced crossflow turbulence and better mixing, offering an effective balance between flow disturbance and surface utilisation. Unlike the 30° layout, which causes excessive pressure drop due to tighter packing, or the 90° layout, which eases flow but limits turbulence, the 45° layout provides moderate ΔP_s while sustaining strong secondary flows. This ensures the best thermal–hydraulic optimisation, with the highest ($h_s/\Delta P_s$) ratio, making it energy-efficient, economically viable, and robust against baffle cut variations in industrial applications.

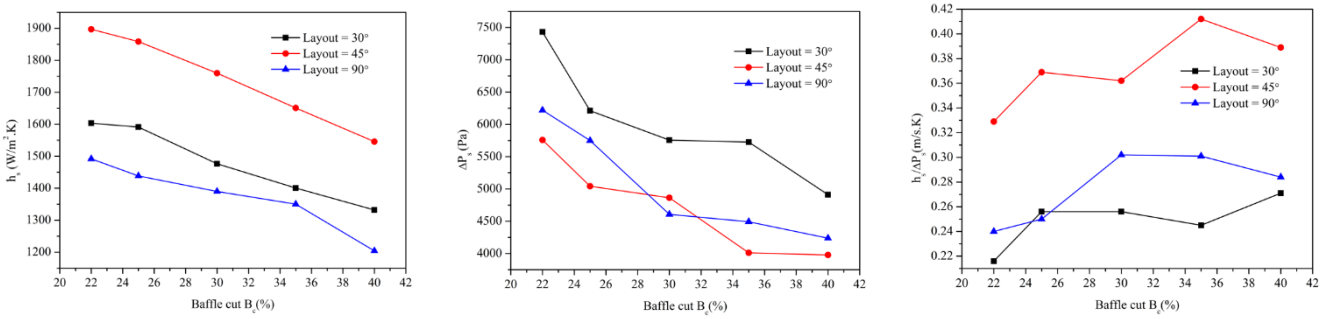

Figure 10. Shows impact of baffle cuts: (a) for h_s, (b) ΔP_s, and (c) the ratio of ($h_s/\Delta P_s$)

4. CONCLUSIONS

In this analysis, the performance of an STHX-SB has been evaluated by adopting the B-D approach for h_s, ΔP_s and the ratio of ($h_s/\Delta P_s$). The B-D method demonstrates optimal fidelity to experimental data. The outcomes reveal that the capability of an STHX is highly dependent on the thermo-physical properties of the fluid, baffle cuts, baffle numbers, tube layouts and mass flow rate. From the findings, the following conclusions have been derived.

i) Although both h_s and ΔP_s increase with the number of baffles in all tube layouts, the ($h_s/\Delta P_s$) ratio decreases correspondingly.

ii) It is noticed that ethylene glycol has the highest h_s for 30° and 45° layouts, but kerosene oil has the highest h_s for 90° layout, though the engine oil has the lowest h_s in all layouts. Similarly, engine oil has the highest and ethylene glycol has the lowest ΔP_s for all tube layouts.

iii) It has also been noticed that from $N_b = 6$ to 12, there is a smooth rise in h_s, but a sharp rise in ΔP_s has been observed for all tube layouts.

iv) It is noticed that at $N_b = 6$, the value of ($h_s/\Delta P_s$) ratio is maximum for all fluids and layouts.

v) It is seen that as the baffle cuts increase, the h_s and ΔP_s decrease for all the layouts.

vi) It is noticed that the highest h_s has been observed for 45° layout while lowest for 90° layout. Further, the ΔP_s is largest for 30° layout and least for 45° layout.

vii) The ratio of ($h_s/\Delta P_s$) is at highest for the 45° layout, followed by the 90° and 30° layouts.

viii) It was found that a baffle cut of $B_c = 35\%$, produce the highest value ($h_s/\Delta P_s$) for the 45° layout. Therefore, 45° layout exhibits more productivity in terms of h_s, ΔP_s and the ratio of ($h_s/\Delta P_s$).

ACKNOWLEDGEMENTS

The authors would like to express their gratitude to Sam Higginbottom University of Agriculture, Technology and Sciences (SHUATS), Prayagraj, India, for offering the technical resources. This study was not supported by any grants from funding bodies in the public, private, or not-for-profit sectors.

CONFLICT OF INTEREST

The authors declare no conflicts of interest that may influence the manuscript.

AUTHORS' CONTRIBUTION

M. Saif (Conceptualizations; Methodology; Writing-Original Draft Preparation; Formal Analysis; Validation)

M. Tariq (Supervision; Conceptualization; Resources; Writing-Reviewing and Editing)

AVAILABILITY OF DATA AND MATERIALS

The datasets generated and/or analysed during the current study are available from the corresponding author on reasonable request.

ETHICS STATEMENT

This study did not involve human participants or animals. Ethical approval was therefore not required.

REFERENCES

[1] S. Kakac, H. L. A. Pramuanjaroenkij, *Heat Exchangers: Selection, Rating, and Thermal Design*, 3rd ed. United States: Taylor & Francis, 2012.

[2] D. P. Sekulić, R. K. Shah, *Fundamentals of Heat Exchanger Design*. United States: John Wiley & Sons, 2023.

[3] K. Thulukkanam, *Heat Exchanger Design Handbook*. United States: CRC Press, 2000.

[4] E. Ozden, I. Tari, "Shell side CFD analysis of a small shell-and-tube heat exchanger," *Energy Conversion and Management*, vol. 51, no. 5, pp. 1004–1014, 2010.

[5] H. Uosofvand, A. A. Abbasian Arani, A. Arefmanesh, "Effect of baffle orientation on shell-and-tube heat exchanger performance," *Journal of Heat and Mass Transfer Research*, vol. 4, no. 2, pp. 83–90, 2017.

[6] M. A. Alperen, E. Kayabaşi, H. Kurt, "Comparison of heat transfer coefficient and pressure loss calculation methods for shell side of shell-and-tube heat exchangers," *Energy Sources, Part A: Recovery, Utilization and Environmental Effects*, vol. 45, no. 2, pp. 5661–5680, 2019.

[7] O. D. Lara-Montaño, F. I. Gómez-Castro, C. Gutiérrez-Antonio, "Comparison of the performance of different metaheuristic methods for the optimization of shell-and-tube heat exchangers," *Computers & Chemical Engineering*, vol. 152, p. 107403, 2021.

[8] Z. Xu, X. Ning, R. Li, X. Wan, C. Zhao, "Configuration optimisation of a shell-and-tube heat exchanger with segmental baffles," *Processes*, vol. 11, no. 11, p. 3152, 2023.

[9] S. Kotian, N. Methekar, N. Jain, P. Vartak, P. Naik, "Thermohydraulic performance evaluation of shell-and-tube heat exchanger using Colburn and Bell–Delaware methods," *Materials Today: Proceedings*, vol. 51, pp. 1051–1054, 2021.

[10] M. A. Jamil, T. S. Goraya, M. W. Shahzad, S. M. Zubair, "Exergoeconomic optimization of a shell-and-tube heat exchanger," *Energy Conversion and Management*, vol. 226, p. 113462, 2020.

[11] S. Alfarawi, "Hydro-thermal shell-side performance evaluation in a shell-and-tube heat exchanger: CFD approach," *Journal of Advanced Research in Fluid Mechanics and Thermal Sciences*, vol. 66, no. 1, pp. 104–119, 2020.

[12] M. Mami, A. Fguiri, M. R. Jeday, "Modeling of BEM type shell-and-tube heat exchanger using the Bell–Delaware method," in *The Proceedings of the 2nd International Conference on Green Energy Conversion Systems (ICGECS 2023)*, Singapore: Springer, 2024, pp. 613–622.

[13] M. Mellal, R. Benzeguir, D. Sahel, H. Ameur, "Hydro-thermal performance of a shell-and-tube heat exchanger under different baffle arrangements," *International Journal of Thermal Sciences*, vol. 121, pp. 138–149, 2017.

[14] A. Aydin, H. Yasar, T. Engin, E. Buyukkaya, "Optimisation and CFD analysis of a shell-and-tube heat exchanger with multi-segmental baffles," *Thermal Science*, vol. 26, no. 1, pp. 1–16, 2022.

[15] A. S. Shukla, K. K. Bhabhor, D. B. Jani, "CFD investigation on shell-and-tube heat exchanger," *International Journal of Advanced Research in Science, Communication and Technology*, vol. 2, no. 5, pp. 239–250, 2022.

[16] K. Anjineyulu, D. K. Mohanty, "Thermo-hydraulic performance analysis of a shell-and-tube heat exchanger with different single segmental baffle configurations," in *Lecture Notes in Mechanical Engineering*, Singapore: Springer, 2023, pp. 335–344.

[17] M. Tayyab, D. A. Awan, A. Shah, "Design optimization of a shell-and-tube heat exchanger based on variable baffle cuts and sizing," *Journal of Thermal Science and Engineering Applications*, vol. 17, no. 2, p. 021008, 2025.

[18] A. P. C. Sarmiento, F. H. Milanese, M. B. H. Mantelli, V. R. Miranda, "Theoretical and experimental studies on two-phase thermosyphon shell and shell heat exchangers," *Applied Thermal Engineering*, vol. 171, p. 115092, 2020.

[19] T. McCaughtry, S. Kim, "Multi-objective optimisation of shell-and-tube heat exchangers using a modified TLBO and compact Bell–Delaware method," *Heat Transfer Engineering*, vol. 43, no. 13, pp. 1083–1096, 2022.

[20] S. Han, X. Li, Z. Liu, B. Zhang, C. He, Q. Chen, "Thermal-economic optimisation of shell-and-tube heat exchanger using improved sparrow search algorithm," *Thermal Science and Engineering Progress*, vol. 45, p. 101923, 2023.

[21] Z. Yang, C. Zhu, Y. Ji, C. Chang, N. Zhang, R. Smith, "Global optimization for the design of shell-and-tube horizontal thermosyphon reboiler," *Energy*, vol. 296, p. 131075, 2024.

[22] P. Prajapati, B. D. Raja, V. Patel, H. Jouhara, "Energy-economic analysis and optimization of a shell-and-tube heat exchanger using a multi-objective heat transfer search algorithm," *Thermal Science and Engineering Progress*, vol. 56, p. 103021, 2024.

[23] Y. You, Y. Chen, M. Xie, X. Luo, L. Jiao, S. Huang, "Numerical simulation and performance improvement for a small size shell-and-tube heat exchanger with trefoil-hole baffles," *Applied Thermal Engineering*, vol. 89, pp. 220–228, 2015.

[24] G. Cucumo, A. Ferraro, D. Kaliakatsos, M. Mele, A. Galloro, R. Schimio, et al., "Thermohydraulic analysis of helical baffle shell-and-tube heat exchanger," *The International Journal of Heat and Technology*, vol. 34, no. 2, pp. S255–S262, 2016.

[25] X. Wang, N. Zheng, Z. Liu, W. Liu, "Shell-side thermal-hydraulic performance of staggered baffle heat exchanger," *International Journal of Heat and Mass Transfer*, vol. 124, pp. 247–259, 2018.

[26] A. A. Abbasian Arani, R. Moradi, "Heat exchanger optimisation using new baffle and tube configuration," *Applied Thermal Engineering*, vol. 157, p. 113745, 2019.

[27] J. Chen, X. Lu, Q. Wang, M. Zeng, "Thermal-hydraulic performance of unilateral ladder-type helical baffle heat exchanger," *Applied Thermal Engineering*, vol. 161, p. 114162, 2019.

[28] H. R. Abbasi, E. Sharifi Sedeh, H. Pourrahmani, M. H. Mohammadi, "Shape optimisation of porous baffles for enhanced performance of shell-and-tube heat exchanger," *Applied Thermal Engineering*, vol. 180, p. 115846, 2020.

[29] D. Wang, H. Wang, J. Xing, Y. Wang, "Thermal-hydraulic characteristics in shell side with quatrefoil perforated plate," *International Journal of Thermal Sciences*, vol. 159, p. 106610, 2021.

[30] M. Saad, A. Munir, M. A. Kamran, "Numerical simulations of shell-and-tube heat exchanger with trefoil and segmented trefoil baffles," *Heat Transfer Engineering*, vol. 44, no. 8, pp. 702–719, 2023.

[31] A. Rahman, W. Winarto, E. Siswanto, "Optimization of shell-and-tube heat exchanger design with inclined baffles," *International Journal of Mechanical Engineering Technologies and Applications*, vol. 5, no. 1, pp. 63–72, 2024.

[32] X. Xiao, X. Zhang, J. Li, B. Jiang, X. Yang, Y. Xia, "Numerical investigation of helical baffle heat exchangers with different Prandtl fluids," *International Journal of Heat and Mass Transfer*, vol. 63, pp. 434–444, 2013.

[33] B. A. Abdelkader. S. M. Zubair, "Performance of shell-and-tube heat exchangers with varying number of baffles," *Heat Transfer Engineering*, vol. 40, no. 1–2, pp. 39–52, 2019.

[34] B. A. Abdelkader, M. A. Jamil, S. M. Zubair, "Thermal-hydraulic characteristics of helical baffle heat exchangers," *Heat Transfer Engineering*, vol. 41, no. 13, pp. 1143–1155, 2020.

[35] M. Saif, M. Tariq, "Effect of operating parameters on the performance of a segmental-baffled shell-and-tube heat exchanger by employing the Bell–Delaware method," *International Journal of Mechanical Engineering and Technology*, vol. 16, no. 5, pp. 41–62, 2025.

[36] A. A. Abd, M. Q. Kareem, S. Z. Naji, "Performance analysis of shell-and-tube heat exchanger: Parametric study," *Case Studies in Thermal Engineering*, vol. 12, pp. 563–568, 2018.

[37] J. Taborek, *Heat Exchanger Design*. United States: CRC Press, 1978.